Optics & Laser Technology 151 (2022) 108044

Contents lists available at ScienceDirect

Optics and Laser Technology

journal homepage: www.elsevier.com/locate/optlastec

Three-dimensional echo distribution analysis of multi-band and oblique Gaussian beams propagating through cat-eye optical system

Zhe Lv [a,b], Xinchen Du [a,b], Kuo Zhang [a,*], Fei Chen [a]

[a] Changchun Institute of optics, Fine Mechanics and Physics, Chinese Academy of Sciences, Changchun 130033, China
[b] University of Chinese Academy of Sciences, Beijing 100049, China

ARTICLE INFO

Keywords:
Cat-eye effect
Multi-band laser active detection
Three-dimensional echo light field

ABSTRACT

The cat-eye effect in optical systems enables active laser detection at long distances and high orientation precision. However, few studies focus on the influence of a multi-band laser with a large incident angle on the echo distribution. This study proposes a three-dimensional echo distribution calculation model of an obliquely incident multi-band laser based on the Collins diffraction integral formula and aperture function expansion as the sum of complex Gaussian functions. The echo distributions for different detection ranges are calculated by coupling the size of the detector in a cat-eye optical system into the model. In the numerical simulation, the influences of laser wavelength, incident angle, and target detector parameter are quantitatively analysed by introducing a target-missing quantity of echo spot and peak light intensity. The results show that the peak light intensity decreases with an increase in incident laser wavelength. When the incident angle increases to a particular value, the peak light intensity decreases sharply, and the target-missing quantity of the echo spot centroid is positively correlated with the incident angle. We can effectively extract important information, such as the working band and detector size, from the cat-eye target echo using this model and provide a trajectory prediction theory for the active detection of a cat-eye target moving at high speed.

1. Introduction

Optical lenses used in photoelectric equipment are typically equipped with reflective or semi-reflective elements at their focal plane [1]. Therefore, when an active detection laser irradiates the target optical system, an echo is reflected from the original path. This effect is called the cat-eye effect, and such a system is called a cat-eye system [2–5]. The cat-eye effect is widely used in free-space optical communications, confocal systems, three-dimensional imaging and adjustment-free lasers [6–9]. The cat-eye system can collimate the detection laser; therefore, the reflected light intensity of the cat-eye system is 2–4 orders of magnitude higher than the general diffuse reflection intensity[10–14]. Thus, laser active detection technology based on the cat-eye effect may realise long-distance target detection.

In the 1980 s, C. Lecocq et al. developed an aiming and positioning system based on the principle of the cat-eye effect [15]. Combining this system with blinding laser weapons can realise accurate aiming and directional confrontation. Researchers from the United States proposed that the principle of the cat-eye effect can be used for laser active detection to search for the optical equipment and photoelectric sensors of enemy targets, determine their working status and position information, and execute accurate attacks and blinding[16]. Recently, there have been some limitations in using the geometric optical ray tracing method to study the echo beam characteristics of the cat-eye optical system. For example, an accurate description of the light field cannot be obtained in the far field, and it is difficult to realise the real-time active detection of high-speed moving cat-eye targets. Therefore, Zhao et al. proposed the use of the Collins diffraction integral formula combined with the aperture function expansion as the sum of complex Gaussian functions to obtain the analytical formula of the echo beam distribution of a cat-eye optical system under far-field conditions [17]. Based on this, Wu et al. introduced the concepts of the optical transmission matrix and combined diffraction aperture to obtain a further cat-eye target echo light field model [18]. For the active detection of cat-eye targets moving at a low speed, He et al. proposed the use of trajectory prediction to achieve the purpose of real-time detection [19].

With the rapid development of intelligent and multifunctional photoelectric equipment, the wavelength bands that are used are diversified, and the detector is complicated. When actively detecting the cat-eye target, it is necessary to effectively collect important information,

* Corresponding author.
E-mail addresses: zhangkuo_fx@163.com (K. Zhang), feichenny@126.com (F. Chen).

https://doi.org/10.1016/j.optlastec.2022.108044
Received 28 November 2021; Received in revised form 13 January 2022; Accepted 4 March 2022
Available online 15 March 2022
0030-3992/© 2022 Elsevier Ltd. All rights reserved.

such as its working band, incident angle, and detector size. However, current research on the influence of wavelength and large-angle oblique-incidence variables in laser active detection using the cat-eye effect is not detailed enough. Additionally, there is a lack of quantitative analysis of the echo spot; therefore, the size information of the cat-eye target detector cannot be effectively obtained. The theory proposed by Liu et al. can only describe the echo light field distribution at a small-angle incidence [20]; however, in practice, the incidence angle of a laser beam entering a cat-eye optical system is relatively large. Zhao et al. proposed that the angle tilt can be converted into a displacement tilt to study the echo light-field distribution at large-angle oblique incidence; however, the propagation process of the detector on the photosensitive surface of the cat-eye target was not considered [21]. In practice, the cat-eye target detector has a significant impact on the echo light field. Therefore, this study makes a unique contribution to current research by establishing a three-dimensional light-field distribution model of the original return of a multi-band Gaussian beam passing through a cat-eye optical system under the condition of a large-angle oblique incidence. The centroid coordinates and target-missing quantity of the echo spot are quantitatively analysed, which provides a theoretical basis for the real-time detection of a cat-eye target moving at high speed.

2. Theoretical derivation of three-dimensional echo light-field distribution

In the large-angle oblique-incidence theoretical model proposed by Zhao [21], the influence of the detector at the photosensitive surface of the cat-eye target is not considered. Therefore, the detector at the photosensitive surface divides the middle optical interval into two, and the three-interval model is expanded into a four-interval model, as shown in Fig. 1. The cat-eye target in the figure is composed of a focusing lens and a plane mirror, and it is symmetrically expanded to convert the reflected light path into a transmitted light path for processing. At this time, the coordinate system is $x'y'z'$, as shown in the figure; the z'-axis is the optical axis direction of the cat-eye optical system, the y'-axis is perpendicular to the z'-axis, and the x'-axis is perpendicular to the paper surface. The incident angle of the detection light θ_y forms a displacement tilt on the cat-eye target detector Δy_2, and the Collins diffraction integral formula is no longer applicable when θ_y is larger.

The coordinate axis is rotated about the direction of the incident light, as shown in Fig. 2; thus, the z-axis denotes the direction of the incident rays. A new coordinate system xyz is established, and the angle tilt at the optical axis is transformed into the displacement tilt. The equivalent aperture at the photosensitive surface of the cat-eye target is transformed from a circular hole hard-edge aperture into an elliptical hole hard-edge aperture, where the displacement tilt Δy_2 is the coordinate value at the centre of the ellipse. At this time, the Collins diffraction integral formula may still be used.

Assuming that the input reference plane is the plane on which the waist radius of the Gaussian beam is ω_0 and the peak intensity on the axis is 1, the light field distribution at the input reference plane can be written as follows:

$$E_0(x_0, y_0) = exp\left(-\frac{x_0^2 + y_0^2}{w_0^2}\right). \tag{1}$$

The cat-eye effect model is decomposed into four optical intervals using matrix optics. The first interval is from the input reference plane to the front mirror of lens 1, which does not contain a hard-edge aperture. The second interval is from the front mirror of lens 1 to the front plane of the detector, which contains the hard-edge aperture of lens 1 (diameter D). The third interval is from the front plane of the detector to the front mirror of lens 2, which contains the hard-edge aperture of the detector (diameter d). The fourth interval is from the front mirror of lens 2 to the output reference plane, which contains the hard-edge aperture of lens 2 (diameter D). Combined with the Collins diffraction integral formula, the optical propagation processes of the four intervals are theoretically deduced.

The transmission matrix of the first interval can be written as

$$\begin{bmatrix} a_1 & b_1 \\ c_1 & d_1 \end{bmatrix} = \begin{bmatrix} 1 & L_1 \\ 0 & 1 \end{bmatrix}, \tag{2}$$

where L_1 is the detection distance from the input reference surface to the cat-eye lens.

Using the Collins diffraction integral formula, the optical field distribution of the emitted beam passing through the first interval to the front mirror of lens 1 can be deduced as follows:

$$E_1(x_1, y_1) = \frac{i}{\lambda b_1} \cdot exp(ikL_1) \cdot \int\int_{-\infty}^{\infty} E_0(x_0, y_0) \cdot exp\left\{ -\frac{ik}{2b_1}\left[a_1\left(x_0^2 + y_0^2\right) - 2(x_0x_1 + y_0y_1) + d_1\left(x_1^2 + y_1^2\right)\right]\right\} dx_1 dy_1. \tag{3}$$

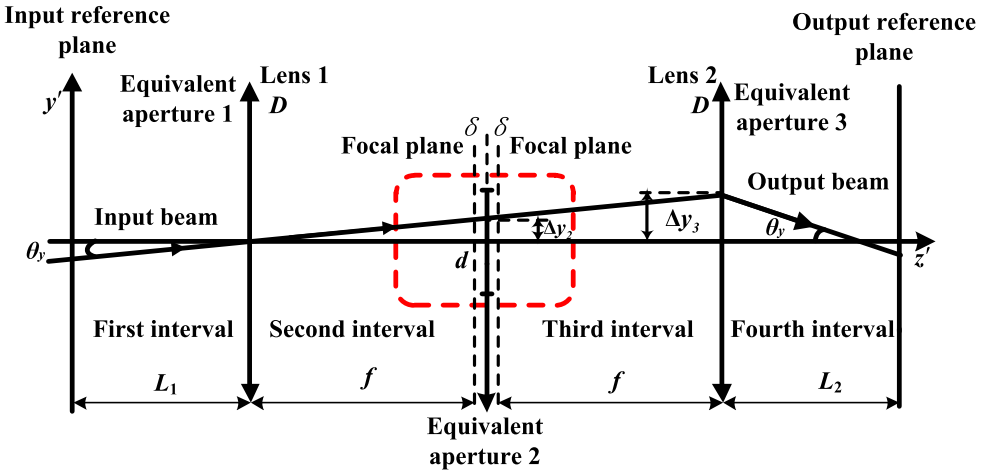

Fig. 1. Cat-eye effect reflection model diagram.

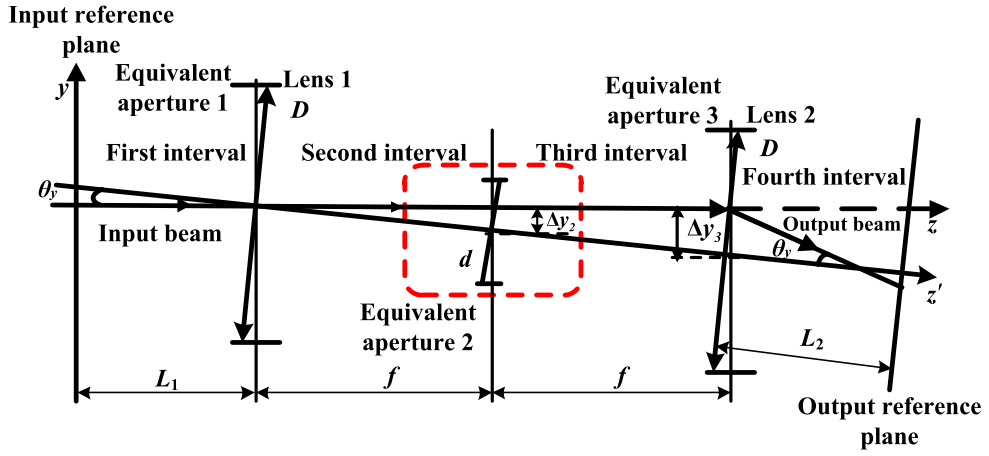

Fig. 2. Cat-eye effect reflection model diagram after coordinate rotation.

Using a special integral formula $\int_{-\infty}^{\infty} exp\left[-\left(P^2x^2+Qx\right)\right]dx = \frac{\sqrt{\pi}}{P}exp\left[\left(\frac{Q}{2P}\right)^2\right]$, the above equation can be expressed as

$$E_1(x_1,y_1)=\frac{ik}{2b_1P_1^2}\cdot\exp(ikL_1)\cdot\exp\left[-\left(\frac{ikd_1}{2b_1}+\frac{k^2}{4b_1^2P_1^2}\right)\cdot\left(x_1^2+y_1^2\right)\right], \tag{4}$$

where

$$k=\frac{2\pi}{\lambda}, P_1^2=\frac{1}{w_0^2}+ik\frac{a_1}{2b_1}. \tag{5}$$

The second interval includes the hard-edge aperture of lens 1 and a range of air transmission distance. Therefore, the interval transfer matrix can be obtained by multiplying the two parts of the matrix. The transmission matrix of the second interval can be written as follows (The second formula is derived from the dispersion formula of thin lens, from which the wavelength variable can be introduced.):

$$\begin{bmatrix} a_2 & b_2 \\ c_2 & d_2 \end{bmatrix}=\begin{bmatrix} 1 & f_0+\delta \\ 0 & 1 \end{bmatrix}\begin{bmatrix} 1 & 0 \\ -\frac{1}{f(\lambda)} & 1 \end{bmatrix}=\begin{bmatrix} 1-\frac{f_0+\delta}{f(\lambda)} & f_0+\delta \\ -\frac{1}{f(\lambda)} & 1 \end{bmatrix},$$

$$f(\lambda)=f_0\cdot\frac{n_0-1}{n(\lambda)-1}, \tag{6}$$

where f_0 and n_0 are the lens focal length and lens refractive index corresponding to the central wavelength of the cat-eye target, respectively, δ is the off-focus of the cat-eye target, and f (λ) and n(λ) are the focal length and refractive index of the cat-eye target lens corresponding to the incident laser wavelength, respectively.

As the emitting beam tilts into the cat-eye target, the shapes of the three equivalent hard-edge apertures become elliptical after the rotation of the coordinate axis. Therefore, the window functions of the three equivalent apertures can be expressed as follows:

$$M_1(x_1,y_1)=\begin{cases} 1, \frac{x_1^2}{\cos^2\theta_x}+\frac{y_1^2}{\cos^2\theta_y}\hat{a}\copyright\frac{1}{2}\left(\frac{D}{2}\right)^2 \\ 0, otherwise \end{cases}$$

$$M_2(x_2,y_2)=\begin{cases} 1, \frac{(x_2-\Delta x_2)}{\cos^2\theta_x}+\frac{(y_2-\Delta y_2)}{\cos^2\theta_y}\hat{a}\copyright\frac{1}{2}\left(\frac{d}{2}\right)^2 \\ 0, otherwise \end{cases} \tag{7}$$

$$M_3(x_3,y_3)=\begin{cases} 1, \frac{(x_3-\Delta x_3)}{\cos^2\theta_x}+\frac{(y_3-\Delta y_3)}{\cos^2\theta_y}\hat{a}\copyright\frac{1}{2}\left(\frac{D}{2}\right)^2 \\ 0, otherwise \end{cases}$$

$$\Delta x_2=-f\cdot\tan\theta_x, \Delta y_2=-f\cdot\tan\theta_y$$

$$\Delta x_3=-2f\cdot\tan\theta_x, \Delta y_3=-2f\cdot\tan\theta_y.$$

where θ_x and θ_y are the oblique angles of the incident laser in the × and y directions, respectively, D is the cat-eye target lens diameter, d is the diameter of the detector at the photosensitive surface of the cat-eye target, and Δx and Δy are the vertical distances between the centre of the equivalent diaphragm and the new z-axis after the rotation of the coordinate axis in the × and y directions, respectively.

The window function of the elliptical hard-edge aperture in equation (7) is approximated by the sum of finite complex Gaussian functions. The expansion formula is as follows:

$$T_1(x_1,y_1)=\sum_{j_1=1}^{M}F_{j_1}exp\left[-\frac{4G_{j_1}}{D^2}\left(\frac{x_1^2}{cos^2\theta_x}+\frac{y_1^2}{cos^2\theta_y}\right)\right]$$

$$T_2(x_2,y_2)=\sum_{j_2=1}^{M}F_{j_2}exp\left\{-\frac{4G_{j_2}}{d^2}\left[\frac{(x_2-\Delta x_2)^2}{cos^2\theta_x}+\frac{(y_2-\Delta y_2)^2}{cos^2\theta_y}\right]\right\} \tag{8}$$

$$T_3(x_3,y_3)=\sum_{j_3=1}^{M}F_{j_3}\exp\{-\frac{4G_{j_3}}{D^2}[\frac{(x_3-\Delta x_3)^2}{\cos^2\theta_x}+\frac{(y_3-\Delta y_3)^2}{\cos^2\theta_y}]\},$$

where F_j and G_j are the expansion coefficients and compound Gaussian coefficients, respectively, and their values can be obtained from Ref. [22] for $M = 10$.

Using the Collins diffraction integral formula, the optical field distribution of the emitted beam at the front plane of the detector through the second interval can be deduced as follows:

$$E_2(x_2,y_2)=\frac{i}{\lambda b_2}\cdot exp(ikf)\cdot\iint_{-\infty}^{\infty}\mathrm{E_1(x_1,y_1)\cdot M_1(x_1,y_1)}\cdot exp\left\{-\frac{\mathrm{ik}}{2\mathrm{b_2}}\left[\mathrm{a_2}\left(\mathrm{x_1^2+y_1^2}\right)-2(\mathrm{x_1x_2+y_1y_2})+\mathrm{d_2}\left(\mathrm{x_2^2+y_2^2}\right)\right]\right\}\mathrm{dx_1dy_1}. \tag{9}$$

The complex Gaussian function expansion of the hard-edge aperture is substituted into equation (9), and the following can be deduced using the special integral formula:

$$E_2(x_2,y_2)=\frac{ik}{2b_1P_1^2}\cdot\frac{ik}{2b_2}\cdot exp[ik(L_1+f)]\cdot\sum_{j_1=1}^{M}\frac{F_{j_1}}{P_{2x}P_{2y}}exp\left[-\frac{k^2}{4b_2^2}\cdot\left(\frac{x_2^2}{P_{2x}^2}+\frac{y_2^2}{P_{2y}^2}\right)\right]exp\left[-\frac{ikd_2}{2b_2}\cdot\left(x_2^2+y_2^2\right)\right], \tag{10}$$

where

$$P_{2x}^2=\frac{ika_2}{2b_2}+\frac{ikd_1}{2b_1}+\frac{k^2}{4b_1^2P_1^2}+\frac{4G_{j_1}}{D^2\cos^2\theta_x}$$

$$P_{2y}^2=\frac{ika_2}{2b_2}+\frac{ikd_1}{2b_1}+\frac{k^2}{4b_1^2P_1^2}+\frac{4G_{j_1}}{D^2\cos^2\theta_y}. \tag{11}$$

The transmission matrix of the third interval can be written as follows:

$$\begin{bmatrix}a_3 & b_3\\ c_3 & d_3\end{bmatrix}=\begin{bmatrix}1 & 0\\ -\frac{1}{f(\lambda)} & 1\end{bmatrix}\begin{bmatrix}1 & f_0+\delta\\ 0 & 1\end{bmatrix}=\begin{bmatrix}1 & f_0+\delta\\ -\frac{1}{f(\lambda)} & 1-\frac{f_0+\delta}{f(\lambda)}\end{bmatrix}. \tag{12}$$

The optical field distribution of the emitted beam as it reaches the front mirror of lens 2 through the third interval can be deduced as follows:

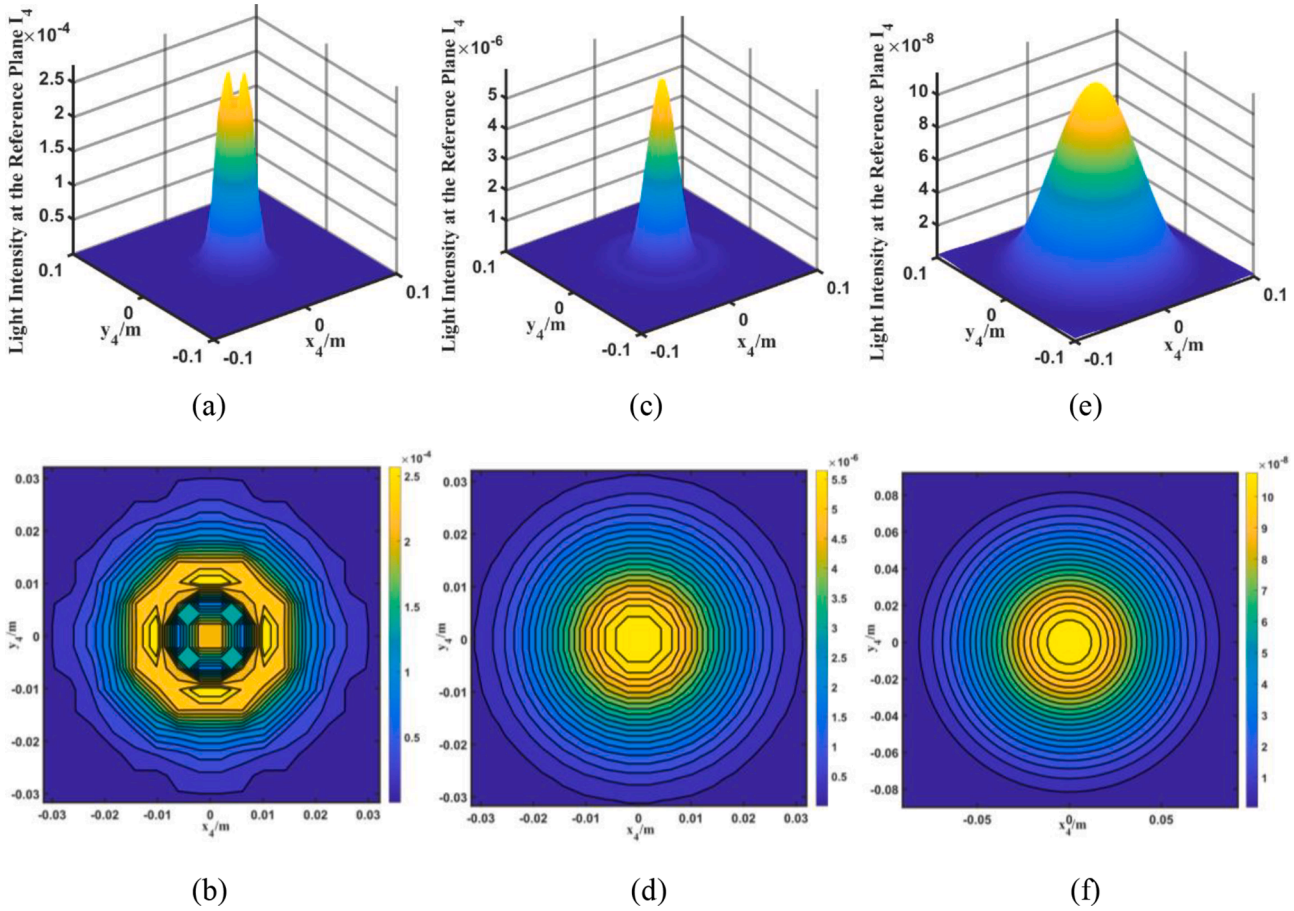

Fig. 3. Three-dimensional distribution and spot distribution of echo light field at different wavelengths (a)(b) λ = 587.6 nm, (c)(d) λ = 3.8 μm, and (e)(f) λ = 10.6 μm.

$$E_3(x_3,y_3)=\frac{i}{\lambda b_3}\cdot\exp(ikf)\cdot\iint_{-\infty}^{\infty}E_2(x_2,y_2)\cdot M_2(x_2,y_2)\cdot\exp\left\{-\frac{ik}{2b_3}\left[a_3\left(x_2^2+y_2^2\right)-2(x_2x_3+y_2y_3)+d_3\left(x_3^2+y_3^2\right)\right]\right\}\mathrm{d}x_2\mathrm{d}y_2. \tag{13}$$

The complex Gaussian function expansion of the hard-edge aperture is substituted into equation (13), and the following can be deduced using the special integral formula:

$$E_3(x_3,y_3)=\frac{ik}{2b_1P_1^2}\cdot\frac{ik}{2b_2}\cdot\frac{ik}{2b_3}\cdot\exp[ik(L_1+2f)]\cdot\exp\left[-\frac{ikd_3}{2b_3}\cdot\left(x_3^2+y_3^2\right)\right]\sum_{j_1=1}^{M}\frac{F_{j_1}}{P_{2x}P_{2y}}\cdot\sum_{j_2=1}^{M}\frac{F_{j_2}}{P_{3x}P_{3y}}\cdot\exp\left[-\frac{4G_{j_2}}{d^2}\cdot\left(\frac{\Delta x_2^2}{\cos^2\theta_x}+\frac{\Delta y_2^2}{\cos^2\theta_y}\right)\right]\cdot\exp\left[-\frac{k^2}{4b_3^2P_{3x}^2}\cdot\left(x_3-\frac{8ib_3G_{j_2}\Delta x_2}{kd^2\cos^2\theta_x}\right)^2\right]\cdot\exp\left[-\frac{k^2}{4b_3^2P_{3y}^2}\cdot\left(y_3-\frac{8ib_3G_{j_2}\Delta y_2}{kd^2\cos^2\theta_y}\right)^2\right], \tag{14}$$

where

$$P_{3x}^2=\frac{ika_3}{2b_3}+\frac{ikd_2}{2b_2}+\frac{k^2}{4b_2^2P_{2x}^2}+\frac{4G_{j_2}}{d^2\cos^2\theta_x}$$

$$P_{3y}^2=\frac{ika_3}{2b_3}+\frac{ikd_2}{2b_2}+\frac{k^2}{4b_2^2P_{2y}^2}+\frac{4G_{j_2}}{d^2\cos^2\theta_y}. \tag{15}$$

The transmission matrix of the fourth interval can be written as

$$\begin{bmatrix}a_4 & b_4\\ c_4 & d_4\end{bmatrix}=\begin{bmatrix}1 & L_2\\ 0 & 1\end{bmatrix}. \tag{16}$$

Using the Collins diffraction integral formula, the light field distribution of the emitted beam at the output reference plane through the fourth interval can be deduced as

$$E_4(x_4,y_4)=\frac{i}{\lambda b_4}\cdot\exp(ikL_2)\cdot\iint_{-\infty}^{\infty}E_3(x_3,y_3)\cdot M_3(x_3,y_3)\cdot\exp\left\{-\frac{ik}{2b_4}\left[a_4\left(x_3^2+y_3^2\right)-2(x_3x_4+y_3y_4)+d_4\left(x_4^2+y_4^2\right)\right]\right\}\mathrm{d}x_3\mathrm{d}y_3 \tag{17}$$

The complex Gaussian function expansion of the hard-edge aperture is substituted into the above equation, and the following can be derived using the special integral formula:

where

$$E_4(x_4,y_4)=\frac{ik}{2b_1P_1^2}\frac{ik}{2b_2}\frac{ik}{2b_3}\frac{ik}{2b_4}\exp[ik(L_1+L_2+2f)]\exp\left[-\frac{ikd_4}{2b_4}\left(x_4^2+y_4^2\right)\right]\sum_{j_1=1}^{M}\frac{F_{j_1}}{P_{2x}P_{2y}}\cdot\sum_{j_2=1}^{M}\frac{F_{j_2}}{P_{3x}P_{3y}}\exp\left[\frac{16G_{j_2}^2}{d^4}\left(\frac{\Delta x_2^2}{P_{3x}^2\cos^4\theta_x}+\frac{\Delta y_2^2}{P_{3y}^2\cos^4\theta_y}\right)\right]\exp\left[-\frac{4G_{j_2}}{d^2}\cdot\left(\frac{\Delta x_2^2}{\cos^2\theta_x}+\frac{\Delta y_2^2}{\cos^2\theta_y}\right)\right]\cdot\sum_{j_3=1}^{M}\frac{F_{j_3}}{P_{4x}P_{4y}}\exp\left[-\frac{k^2}{4b_4^2P_{4x}^2}\left(x_4-\frac{8ib_4G_{j_3}\Delta x_3}{kD^2\cos^2\theta_x}+\frac{4b_4G_{j_2}\Delta x_2}{b_3P_{3x}^2d^2\cos^2\theta_x}\right)^2\right]\cdot\exp\left[-\frac{k^2}{4b_4^2P_{4y}^2}\left(y_4-\frac{8ib_4G_{j_3}\Delta y_3}{kD^2\cos^2\theta_y}+\frac{4b_4G_{j_2}\Delta y_2}{b_3P_{3y}^2d^2\cos^2\theta_y}\right)^2\right]\exp\left[-\frac{4G_{j_3}}{D^2}\left(\frac{\Delta x_3^2}{\cos^2\theta_x}+\frac{\Delta y_3^2}{\cos^2\theta_y}\right)\right], \tag{18}$$

$$P_{4x}^2=\frac{ika_4}{2b_4}+\frac{ikd_3}{2b_3}+\frac{k^2}{4b_3^2P_{3x}^2}+\frac{4G_{j_3}}{D^2\cos^2\theta_x}$$

$$P_{4y}^2=\frac{ika_4}{2b_4}+\frac{ikd_3}{2b_3}+\frac{k^2}{4b_3^2P_{3y}^2}+\frac{4G_{j_3}}{D^2\cos^2\theta_y}. \tag{19}$$

Therefore, the light intensity distribution at the output reference plane can be written as follows:

$$I_4(x_4,y_4)=E_4(x_4,y_4)\cdot E_4^*(x_4,y_4). \tag{20}$$

3. Numerical simulation and discussion of echo light field

Based on analytical formula (20), the specific distribution of the three-dimensional echo light field of a cat-eye optical system under different wavebands, different large-angle incidence angles, and different detection distances can be completely described. In the numerical calculation, the initial values are set as follows: the focal length of the cat-eye target lens is 100 mm, the diameter of the aperture is 25.4 mm, the diameter of the detector at the focal plane is 10 mm, and the defocus is zero. Assuming that the peak intensity on the axis at the waist of the incident beam is 1, the simulation results are the relative values of the light intensity. The numerical simulation primarily considers the effects of the wavelength of the incident light and the large angle of incidence on the echo light-field distribution of the cat-eye optical

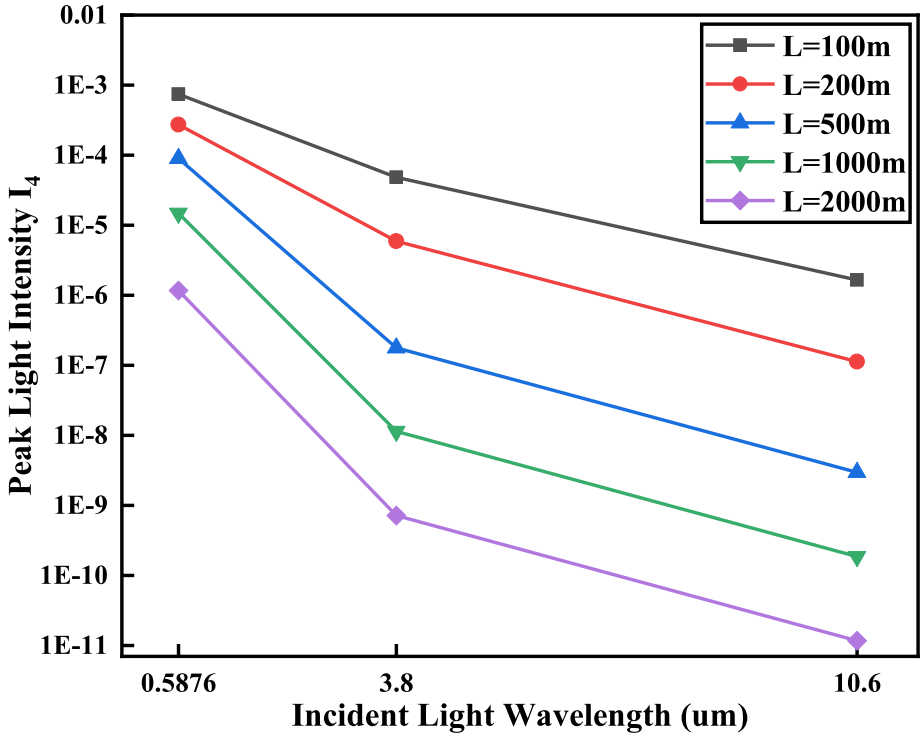

Fig. 4. Relationship between incident-light wavelength and peak light intensity of echo light field at different detection distances.

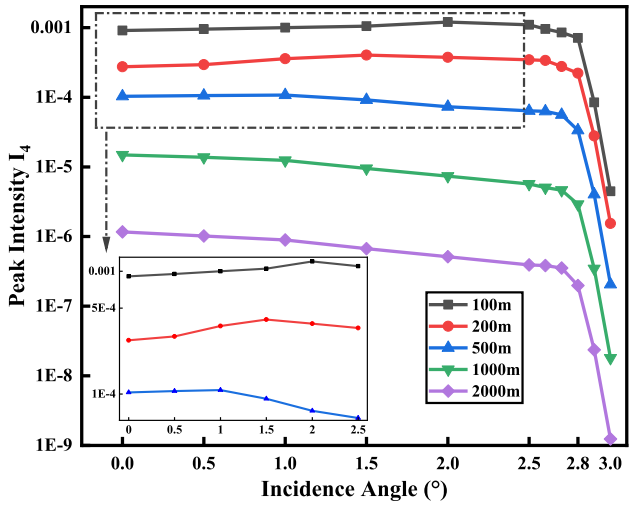

Fig. 5. Relationship between the incident angle of the light and the peak light intensity of the echo light field at different detection distances.

system.

3.1. *Influence of incident light wavelength on echo light-field distribution*

Previous research shows that after detection light of different bands enters the cat-eye target, the actual focal length will change towing to the different wavelengths; therefore, the defocus is introduced to change the echo light-field distribution. However, the influence of the change in wavelength itself has not been studied. The different wavelengths of incident light change the diffraction limit, which change the diffraction effect and diffraction field broadening in the process of beam propagation. In the numerical simulation, the material of the cat-eye target lens is changed, such that the wavelength of the incident light is always the centre wavelength of the cat-eye target lens, and the defocus caused by the wavelength change is maintained at zero. The cat-eye target lens materials are fused quartz, MgF_2, and ZnSe. The central band and incident light wavelengths are 587.6 nm for visible light, 3.8 μm for medium-wave light, and 10.6 μm for long-wave light. The focal length of the cat-eye lens corresponding to the central band is 100 mm.

The formula for the diffraction limit Airy-spot diameter is

$$D_A = 2.44 \cdot \frac{\lambda}{D_H} \cdot L, \tag{21}$$

where D_A is the Airy-spot diameter, and D_H is the effective diffraction aperture of the cat-eye target. When the detection laser is transmitted into the cat's eye target after a certain distance, the actual diffraction aperture will change due to the change of the incident angle, not the lens aperture, so it is necessary to introduce D_H. The schematic diagram is shown in Fig. 6 in 3.2.2. From this formula, when the wavelength

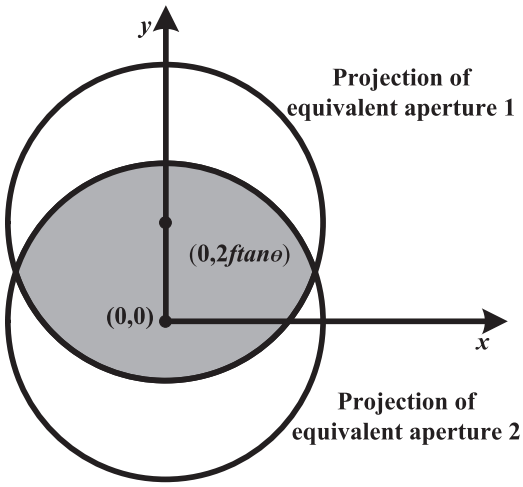

Fig. 6. Schematic of effective diffraction aperture of cat-eye target.

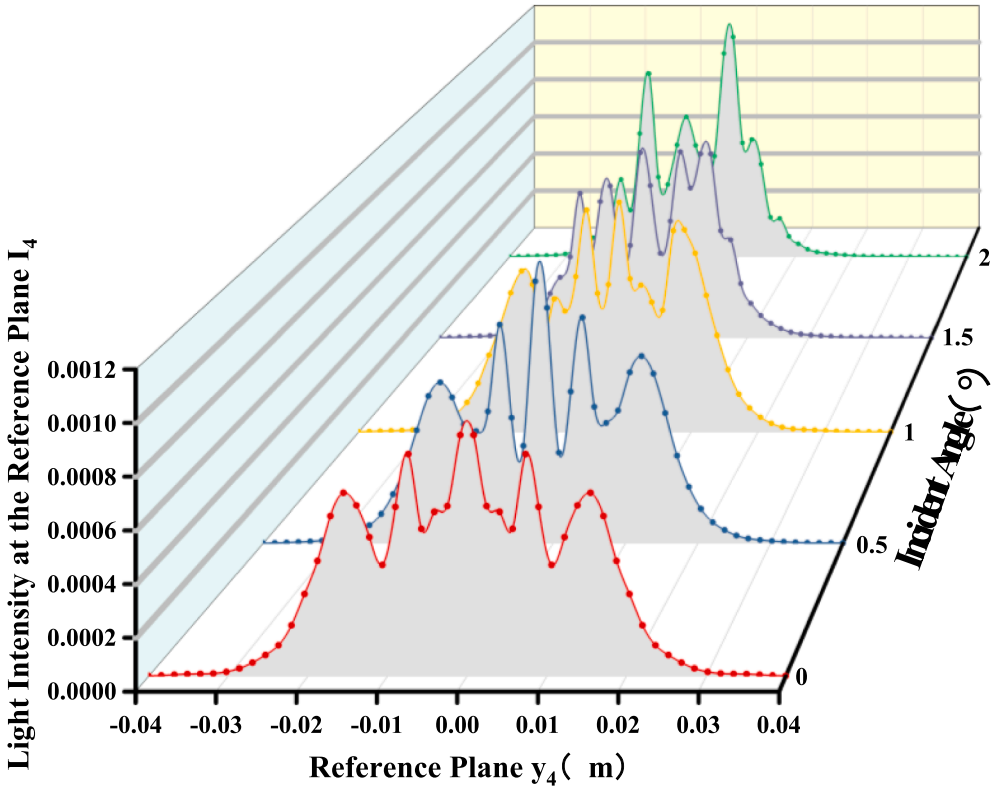

Fig. 7. Relationship between the incident angle and y–z plane of the echo light field at L = 100 *m*.

increases, the diffraction limit increases, and the diameter of the Airy spot increases. Fig. 3 shows the light-field distribution diagrams of the incident light of different central bands returning to the receiving reference plane along the original path after entering the cat-eye target when the detection distance L is 200 m. Comparing the echo light-field distribution patterns of the three central bands, it can be observed that with an increase in the incident-light wavelength, the central energy gradually diffuses outward. Additionally, the echo-spot diameter increases, which corresponds to the Airy-spot diameter formula.

The relationship between the incident light wavelength and the peak light intensity of the echo light field when the diffraction limit is the main influencing factor is shown in Fig. 4 for different detection distances. It is intuitively inferred from the figure that the peak light intensity of the echo light field decreases with an increase in the incident light wavelength. This occurs because an increase in the incident-light wavelength causes increases in the diffraction effect and echo-spot diameter; thus, the echo energy diffuses outward, and the peak light intensity decreases gradually. According to the investigation, it is first proposed that the incident-light wavelength has a particular corresponding relationship with the echo peak light intensity because it affects the diffraction limit. Using this relationship and the detection distance, an analysis of the echo light-field distribution can effectively obtain the working-band information of the cat-eye target.

3.2. *Influence of large incident angle on echo light-field distribution*

The effects of the incident angle on the echo peak light intensity, echo light-field distribution, and target-missing quantity of the echo spot are primarily considered in the numerical simulation. The relevant variables are set as follows: the central wavelength of the cat-eye target and the wavelength of the incident light is 587.6 nm, the focal length of the cat-eye target lens is 100 mm, its aperture diameter is 25.4 mm, the diameter of the detector at the focal plane is 10 mm, the detection distance L is between 100 m and 2000 m, the incident angle of the light θ_y increases gradually from 0° to 3°, and θ_x is zero.

3.2.1. *Influence of incident angle on echo peak intensity*

The peak light intensities of the echo light field under different detection distances and different incident angles are extracted, and the corresponding relationship diagram is shown in Fig. 5. The inset of the figure is a partially enlarged view of the dotted portion. It is observed from the local enlarged view that the maximum peak light intensity at a short distance occurs when there is a finite incident angle, not when the incident angle is zero in the geometric optics method; this is consistent with the description in Ref. [23]. From the simulation model diagram, it can be further observed that with an increase in the detection distance, the angle of the maximum peak light intensity gradually decreases. After reaching a particular distance, the maximum peak light intensity appears when the incident angle is zero. This is due to the competitive effect of the incident angle and detection distance on the diffraction effect. The specific explanation of the influence of the incident angle on the echo light field distribution is given in section 3.2.2.

According to formula (7), when the incident angle is 2.9°, the displacement tilt Δy_2, which is introduced by the angle inclination at the

Table 1
Target-missing quantity values of the echo spot corresponding to different detection distances and incident angles.

Target-missing quantity (m)		Detection distance (m)				
		100	200	500	1000	2000
Incident angle (°)	0	0	0	0	0	0
	0.5	0.0011	0.0015	0.0015	0.0014	0.0016
	1	0.0024	0.0030	0.0031	0.0030	0.0033
	1.5	0.0038	0.0046	0.0047	0.0046	0.0049
	2	0.0054	0.0063	0.0061	0.0061	0.0065
	2.5	0.0071	0.0079	0.0076	0.0078	0.0081
	3	0.0086	0.0095	0.0091	0.0093	0.0094

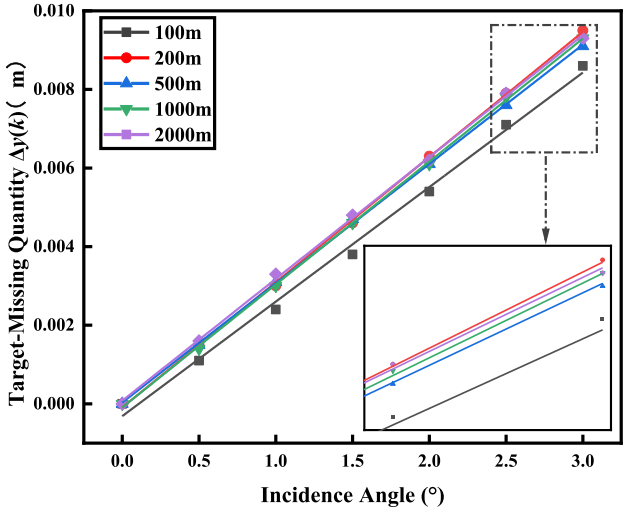

Fig. 8. Relationship between incident angle and spot centroid target-missing quantity.

photosensitive surface of the cat-eye target, is approximately 5.06 mm; this is slightly larger than the 5 mm radius of the detector at the photosensitive surface. At this time, most of the energy of the incident light does not enter the cat-eye target. Therefore, the echo light intensity on the receiving plane will also be very weak, which is consistent with the rapid reduction of the peak light intensity at the incident angle of 2.9° under different detection distances in Fig. 5. In the practical active detection of the cat-eye target, this conclusion can be used to obtain the relevant information of the size of the cat-eye target detector from the echo light field. The size of the detector at the photosensitive surface of the detected cat-eye target can be retrieved by obtaining the incident angle corresponding to the sudden decrease in the echo light intensity. This study proposes a novel solution to effectively obtain the size information of the cat-eye target detector in the active detection of the cat-eye target.

3.2.2. *Influence of incident angle on echo light field distribution*

In Fig. 2, equivalent aperture 1 is projected onto equivalent aperture 2 along the direction of the incident light. The overlapping part of the two apertures is the effective diffraction aperture of the cat-eye target, as shown in the shaded part of Fig. 6. The effective diffraction aperture D_H decreases gradually with an increase in the incident angle θ_y.

Because the tilt effects in the × and y directions are consistent, only the change law of the incident angle in the y direction is studied. The y–z plane distribution of the echo light field at different incident angles of L = 100 m is extracted, as shown in Fig. 7. Theoretical analysis shows that with an increase in the incident angle θ_y, the effective diffraction aperture of the cat-eye target decreases, the profile of the light-field distribution gradually decreases, the diffraction peak gradually decreases, the main diffraction peak light intensity gradually shifts to the secondary diffraction peak light intensity, and the highest peak begins to increase slowly. This is consistent with the y–z plane distribution of the echo light field at different incident angles when L = 100 m in Fig. 7. However, with a gradual increase in the detection distance, the diffraction effect increases sharply, and the broadening speed of the diffraction light field is greater than that of the diffraction peak. Therefore, the incidence angle when the peak light intensity reaches its maximum gradually decreases. Additionally, when the peak light intensity reaches its maximum after a particular distance, the incidence angle is zero, which is consistent with the description in section 3.2.1. This also shows that the theoretical model is self-consistent.

3.2.3. *Influence of incident angle on target-missing quantity of echo spot*

The definitions of the spot-centroid coordinates and spot target-missing quantity are introduced to quantitatively analyse the echo spot pattern. The spot-centroid coordinates are given by the first-order moment of the spot data. The absolute value of the centroid difference of the echo spot at different incident angles and zero degrees is defined as the spot target-missing quantity. The definition formulas are as follows:

$$x(k) = \frac{\sum_{j=1}^{m}\sum_{i=1}^{n} x_{ij} I_{ij}(k)}{\sum_{j=1}^{m}\sum_{i=1}^{n} I_{ij}(k)} y(k) = \frac{\sum_{j=1}^{m}\sum_{i=1}^{n} y_{ij} I_{ij}(k)}{\sum_{j=1}^{m}\sum_{i=1}^{n} I_{ij}(k)}$$

$$\Delta x(k) = |x_0(k) - x_\theta(k)\,|\Delta y(k) = |y_0(k) - y_\theta(k)\,|, \tag{22}$$

where $x(k)$ and $y(k)$ are the transverse and longitudinal coordinates of the spot centroid, respectively, n and m are the number of pixels in the × and y directions of the receiving plane, respectively, x_{ij} and y_{ij} are the x- and y-coordinate values corresponding to the number of pixels in the receiving plane, respectively, $I_{ij}(k)$ are the light intensity values corresponding to the pixels, $y_0(k)$ and $y_\theta(k)$ are the ordinate of the spot centroid corresponding to 0° and θ° incident angles, respectively, and $\Delta x(k)$ and $\Delta y(k)$ are the target-missing quantities in the × and y directions, respectively.

This study only considers incidence at different angles in the y direction, and the × direction is similar. Therefore, the target-missing quantity data of the echo spot in the y direction at different detection distances and different incidence angles are obtained, as shown in Table 1.

The data in Table 1 are linearly fitted, as shown in Fig. 8. The inset of the figure is an enlarged view of the dotted box. It can be observed from the figure that the target-missing quantity of the echo spot centroid is positively correlated with the incident angle, its slope is only related to the parameters of the cat-eye target itself, and the detection distance only changes its intercept. This provides a theoretical basis for trajectory prediction in the active detection of a cat-eye target moving at high speed, and it provides continuous tracking and active detection in real time.

4. Conclusions

We proposed a three-dimensional echo-distribution calculation model for a multi-band laser obliquely incident on a cat-eye target. The focal length dispersion formula is introduced into the optical transmission matrix to calculate the influence of the incident-light wavelength on the performance of the laser active detection. By considering the target detector in the model, the influence of the size of the target detector on the echo distribution can be effectively obtained. The numerical simulation primarily considers the influences of the incident laser wavelength and angle on the echo light field of the cat-eye target, and the target-missing quantity of the echo spot and the peak light intensity were obtained for quantitative analysis. The results show that the peak light intensity decreases with an increase in the incident laser wavelength. When the incident angle increases to a particular value, the peak light intensity decreases sharply, and the target-missing quantity of the echo spot centroid is positively correlated with the incident angle. The theoretical model in this study provides a new method to obtain the target working band and target detector size for laser active detection, and it offers a trajectory-prediction theory for the laser active detection of cat-eye targets moving at high speed. However, there are some limitations in the work of this paper. For example, the cat-eye target is composed of a focusing lens and a plane mirror in this model, but the real cat's eye target is not made up of this. In the future work, we will use the actual CCD instead of the simple cat's eye target model. And the influence of atmospheric turbulence on light wave propagation will be considered.

5. Funding sources

National Natural Science Foundation (61904178), Innovation Cross team of the Chinese Academy of Sciences (JCTD-2020–13), Member of the Youth Innovation Promotion Association of the Chinese Academy of Sciences (2020227), Funding of 'Xuguang Talents' from CIOMP

Declaration of Competing Interest

The authors declare that they have no known competing financial interests or personal relationships that could have appeared to influence the work reported in this paper.

References

[1] Y.-Z. Zhao, H.-Y. Sun, Y.-H. Zheng, C.-M. Shan, Y.-C. Fan, An interferometry measure method on vibration spectrum of optical target based on cat-eye effect[J], Opt. Laser Technol. 58 (2014) 1–7, https://doi.org/10.1016/j.optlastec.2013.10.029.

[2] M. Gong, S. He, Periodicity analysis on cat-eye reflected beam profiles of optical detectors[J], Opt. Eng. 56 (5) (2017) 053110, https://doi.org/10.1117/1.OE.56.5.053110.

[3] Y.Z. Zhao, H.Y. Sun, C.M. Shan, Y.H. Zheng, L.X. Zhang, A new identification method aimed at optical targets using an active interference laser beam[J], IEEE Photon Technol. Lett. 26 (10) (2014) 1019–1022, https://doi.org/10.1109/LPT.2014.2312382.

[4] J. Huang, H. Zhang, L. Wang, Z. Zhang, C. Zhao, Improved YOLOv3 Model for miniature camera detection [J], Opt. Laser Technol. 142 (2021) 107133.

[5] M. Gong, S. He, R. Guo, W. Wang, Cat-eye effect reflected beam profiles of an optical system with sensor array[J], Appl. Opt. 55 (16) (2016) 4461, https://doi.org/10.1364/AO.55.004461.

[6] M. Portnoi, P.A. Haigh, T.J. Macdonald, F. Ambroz, I.P. Parkin, I. Darwazeh, I. Papakonstantinou, Bandwidth limits of luminescent solar concentrators as detectors in free-space optical communication systems[J], Light Sci. Appl. 10 (1) (2021), https://doi.org/10.1038/s41377-020-00444-y.

[7] T. Liu, M. Rajadhyaksha, D.L. Dickensheets, MEMS-in-the-lens architecture for a miniature high-NA laser scanning microscope[J], Light Sci. Appl. 8 (1) (2019) 59, https://doi.org/10.1038/s41377-019-0167-5.

[8] Z.-B. Fan, H.-Y. Qiu, H.-L. Zhang, X.-N. Pang, L.-D. Zhou, L. Liu, H. Ren, Q.-H. Wang, J.-W. Dong, A broadband achromatic metalens array for integral imaging in the visible[J], Light Sci. Appl. 8 (1) (2019), https://doi.org/10.1038/s41377-019-0178-2.

[9] Z. Cao, X. Zhang, G. Osnabrugge, J. Li, I.M. Vellekoop, A.M.J. Koonen, Reconfigurable beam system for non-line-of-sight free-space optical communication[J], Light Sci. Appl. 8 (1) (2019), https://doi.org/10.1038/s41377-019-0177-3.

[10] S. He, M. Gong, Optimized phase mask to realize retro-reflection reduction for optical systems[J], J. Opt. 19 (10) (2017) 105610, https://doi.org/10.1088/2040-8986/aa8606.

[11] Y.-Z. Zhao, H.-Y. Sun, L.-X. Zhang, Y.-H. Zheng, Light intensity at the return place and encirclement power ratio for the distorted reflected beam based on cat-eye effect[J], Optoelectron. Lett. 7 (6) (2011) 478–482, https://doi.org/10.1007/s11801-011-1055-2.

[12] Czarske J, Zhang S, Sampson D, et al. The simulation study on optical target laser active detection performance[C]. International Symposium on Optoelectronic Technology & Application: Laser & Optical Measurement Technology & Fiber Optic Sensors. International Society for Optics and Photonics, 2014:929724.

[13] M.X. Zhang, Y. Lv, X.Y. Li, R. Geng, L.G. Sheng, Theoretical analysis on retro-reflected wave power based on "cat-eye" effect in defocusing condition[J], Appl. Mech. Mater. 644-650 (2014) 1342–1345, https://doi.org/10.4028/www.scientific.net/AMM.644-650.1342.

[14] S. He, M. Yuan, M. Gong, Freeform lens design to eliminate retroreflection for optical systems[J], Appl. Opt. 57 (2018) 1218–1224, https://doi.org/10.1364/AO.57.001218.

[15] H.Y. Sun, Y.Z. Zhao, Y.H. Zheng, Research and application of laser active detection technology based on cat's eye effect [J], J. Equip. Acad. 23 (2012) 6–13, in Chinese.

[16] Y.Z. Zhao, H.Y. Sun, F.H. Song, et al., Research status and development trend of cat's eye effect in laser active detection technology [J], Progr. Laser Optoelectron. 47 (2010) 38–47, in Chinese.

[17] Y.Z. Zhao, H.Y. Sun, F.H. Song, et al., A physical optical transmission analysis method for studying the cat's eye effect of optical lens [J], J. Inst. Equip. Command Technol. 57 (2008) 2284–2294, in Chinese.

[18] D.S. Wu, B.Q. Liu, W.G. Hu, et al., Echo characteristic model of cat's eye effect based on matrix optics [J], J. Opt. 36 (2016) 92–98, in Chinese.

[19] S. He, M. Yuan, M. Gong, Active laser detection system for recognizing surveillance devices[J], Opt. Commun. 426 (2018) 313–324, https://doi.org/10.1016/j.optcom.2018.05.069.

[20] B.Q. Liu, B. Zhou, D.S. Wu, et al., Dual-channel active laser detection system[J], Opt. Precision Eng. 20 (2012) 241–246, in Chinese.

[21] Y.Z. Zhao, H.Y. Sun, Y.H. Zheng, An approximate analytical propagation formula for Gaussian beams through a cat-eye optical lens under large incidence angle condition[J], Chin. Phys. Lett. 28 (2011) 074101–74837, https://doi.org/10.1088/0256-307X/28/7/074101.

[22] J.J. Wen, M.A. Breazeale, A diffraction beam field expressed as the superposition of Gaussian beams[J], J. Acoust. Soc. Am. 83 (1988) 1752–1756, https://doi.org/10.1121/1.396508.

[23] Z. Yan-Zhong, S. Hua-Yan, Y.u. Xia-Qiong, F. Meng-Shan, Three-dimensional analytical formula for oblique and off-axis gaussian beams propagating through a cat-eye optical lens, Chinese Phys. Lett. 27 (3) (2010) 034101.